Large Excitonic Reflectivity of Monolayer MoSe_{2} Encapsulated in Hexagonal Boron Nitride

Giovanni Scuri, You Zhou, Alexander A. High, Dominik S. Wild, Chi Shu, Kristiaan De Greve, Luis A. Jauregui, Takashi Taniguchi, Kenji Watanabe, Philip Kim, Mikhail D. Lukin, and Hongkun Park

Phys. Rev. Lett. **120**, 037402 — Published 18 January 2018

DOI: 10.1103/PhysRevLett.120.037402

Large excitonic reflectivity of monolayer $MoSe_2$ encapsulated in hexagonal boron nitride

Giovanni Scuri[1†], You Zhou[1,2†], Alexander A. High[1,2†], Dominik S. Wild[1†], Chi Shu[1], Kristiaan De Greve[1,2], Luis A. Jauregui[1], Takashi Taniguchi[3], Kenji Watanabe[3], Philip Kim[1*], Mikhail D. Lukin[1*] & Hongkun Park[1,2*]

[1]Department of Physics and [2]Department of Chemistry and Chemical Biology, Harvard University, Cambridge, MA 02138, USA

[3]National Institute for Materials Science, 1-1 Namiki, Tsukuba 305-0044, Japan

†These authors contributed equally to this work.

*To whom correspondence should be addressed: hongkun_park@harvard.edu, lukin@physics.harvard.edu, pkim@physics.harvard.edu

We demonstrate that a single layer of $MoSe_2$ encapsulated by hexagonal boron nitride can act as an electrically switchable mirror at cryogenic temperatures, reflecting up to 85% of incident light at the excitonic resonance. This high reflectance is a direct consequence of the excellent coherence properties of excitons in this atomically thin semiconductor. We show that the $MoSe_2$ monolayer exhibits power- and wavelength-dependent nonlinearities that stem from exciton-based lattice heating in the case of continuous-wave excitation and exciton-exciton interactions when fast, pulsed laser excitation is used.

Mirrors are ubiquitous elements of optical and optoelectronic circuits. Their miniaturization is fundamentally limited by the optical wavelength in the case of dielectric mirrors and photonic crystals [1] or the skin depth for metallic mirrors [2]. Recently, resonant scattering has emerged as a method for overcoming these limitations and for controlling light at the atomic scale [3-11]. For instance, highly reflective mirrors based on individual quantum emitters have been demonstrated by coupling them to optical cavities and nanophotonic waveguides [3-8]. Such resonant mirrors feature unusual properties due to their extraordinary nonlinearity down to the single-photon level [3-8]. A two-dimensional (2D) layer of emitters, such as atomic lattices or excitons [9-11], has also been predicted to act as an efficient mirror when the incident light is resonant with the resonance frequency of the system. Such atomically thin mirrors represent the ultimate miniaturization limit of a reflective surface, and could enable unique applications ranging from quantum nonlinear optics [9-11] to topological photonics [12,13].

In this Letter, we demonstrate that transition metal dichalcogenide (TMD) monolayers can act as atomically thin, electrically switchable, resonant mirrors. These materials are direct-bandgap semiconductors that support tightly bound excitons. Excitonic transitions in TMD monolayers exhibit large oscillator strengths [14-16], resulting in large radiative linewidths compared to excitons in other semiconductor systems. In addition, the excitonic response in monolayers can be controlled electrically via gate-induced doping [17-21]. Importantly, these monolayers can be easily integrated with other 2D materials via van der Waals stacking to improve their quality or add new functionalities. One of the most studied amongst such heterostructures is a TMD monolayer encapsulated by two hexagonal boron nitride (hBN) flakes: this “passivated” monolayer exhibits enhanced carrier mobility [21,22] and reduced photoluminescence linewidth [23-25].

Our experiments employ a device that consists of an hBN-passivated $MoSe_2$ monolayer placed on an oxide-covered Si substrate, and we measure its reflectance with a normally incident laser beam (Figs. 1(a) and 1(b)). The doped Si substrate is used as a gate electrode: by applying a gate voltage (V_g), $MoSe_2$ monolayers can be made intrinsic or *n*-doped. When a monochromatic laser beam is tuned to the exciton resonance, we observe substantial reflection from a monolayer device (**M1)** at $V_g < 10$ V at $T = 4$ K (Fig. 1(c)). The reflection contrast between the monolayer region and the substrate disappears at $V_g > 20$ V (Fig. 1(d)), indicating that the reflection can be turned off electrically. When we illuminate another monolayer device **(M2)** with a supercontinuum laser and spectrally resolve the reflection, we find that both the magnitudes and wavelength positions of the reflectance peaks change with V_g (Fig. 1(e)). We obtain the absolute reflectance value of a TMD heterostructure by comparing its wavelength dependent reflectance to that of a thick gold layer (assumed to be a perfect reflector for the relevant wavelength range) or the SiO_2 substrate (with known frequency-dependent reflectance). When the monolayer is intrinsic ($V_g < 10$ V), the reflection is dominated by a peak at the wavelength of the neutral exciton transition. When $MoSe_2$ is *n*-doped ($V_g > 20$ V), however, the reflection by the neutral exciton disappears, and a new, weaker, reflectance peak appears at the charged exciton resonance [17,19,21]. These observations are consistent with previous studies [17,19] that showed the disappearance (appearance) of the neutral (charged) exciton absorption in the *n*-doped region.

Figure 2(a) shows temperature-dependent reflectance spectra. At $T = 4$ K, the peak reflectance value reaches 0.8, demonstrating that the device can act as an efficient resonant mirror. The reflectance lineshape is not Lorentzian but rather asymmetric, exhibiting both a minimum and maximum near the neutral exciton resonance, consistent with previous differential reflectance measurements [18,26-30]. As temperature increases, peak reflectance decreases while

the linewidth increases. The peak reflectance value varies in different samples or even within the same monolayer at distinct spatial locations, typically ranging from ~0.5 to 0.8. Some of these variations may stem from the intrinsic heterogeneity of the material (e.g. defects in the crystal) or charge/strain inhomogeneity introduced during the fabrication process. We note that these absolute reflectance values are significantly higher than those reported previously via both absolute [31] and differential reflectance measurements of TMDs [18,26-30].

In order to gain insight into our observations in Fig. 2(a), we first consider the response of a free-standing $MoSe_2$ monolayer to normally incident coherent light, tuned close to the exciton resonance. Because only a single exciton resonance is relevant over the frequency range of interest, the susceptibility of a $MoSe_2$ monolayer can be described by the Lorentzian function [32,33]:

$$\chi(\omega) = -\frac{c}{\omega_0 d}\frac{\gamma_r}{\omega - \omega_0 + i\gamma_{nr}/2}, \quad (1)$$

where ω_0 denotes the exciton resonance (angular) frequency, d is the thickness of the monolayer, and γ_r and γ_{nr} and are the radiative and non-radiative decay rates of the exciton, respectively. For simplicity, we ignored the background susceptibility of $MoSe_2$ since it only weakly affects the reflectance [34]. In the relevant limit $\omega_0 d/c \ll 1$, the reflectance of the monolayer is given by:

$$R(\omega) = \frac{\gamma_r^2/4}{(\omega - \omega_0)^2 + (\gamma_r + \gamma_{nr})^2/4}. \quad (2)$$

On resonance, the reflectance reaches the maximum value $R(\omega_0) = \gamma_r^2/(\gamma_r + \gamma_{nr})^2$. Hence, reflectance is a direct measure of the radiative rate of the exciton transition, γ_r, relative to the total rate $\gamma_r + \gamma_{nr}$. In the absence of non-radiative ($\gamma_{nr} = 0$) and disorder-induced broadening [34],

the peak reflectance becomes unity, and the monolayer acts as a perfect mirror. This effect is caused by destructive interference of the incident light with the optical field generated by the excitons, resulting in suppressed transmission and enhanced reflection [11]. The reflectance may alternatively be understood in terms of the sheet conductivity $\sigma_s(\omega) = -i\varepsilon_0\omega d\chi(\omega)$ [31]. On resonance, the real part is given by $\mathrm{Re}[\sigma_s(\omega_0)] = G_0/(2\alpha)(\gamma_r/\gamma_{nr})$, where $G_0 = 2e^2/h$ is the conductance quantum and α is the fine-structure constant. The sheet conductivity diverges as $\gamma_{nr} \to 0$, leading to a large impedance mismatch between the monolayer and free space, which in turn gives rise to high reflectance.

The presence of proximal dielectrics and other reflectors considerably modifies the optical response. The lineshape shown in Fig. 2(a) originates from the interference between the $MoSe_2$ and substrate reflections. In our device, the $MoSe_2$ monolayer is embedded in a dielectric stack of hBN, SiO_2, and Si that acts as a multilayer broadband reflector (inset of Fig. 2(a)). Because the phase of the light reflected by the $MoSe_2$ monolayer varies by π across the resonance, the interference between $MoSe_2$ reflection and substrate reflection produces an asymmetric lineshape (Fig. 2(a)). As such, the entire hBN/$MoSe_2$/hBN/SiO_2/Si heterostructure forms an effective cavity, confining the optical field between the resonant $MoSe_2$ mirror and a broadband reflector, which can strongly modify the radiative decay of the excitonic system compared to its value in free space [39]. As discussed in [34], for the present devices, the decay rate is reduced by a factor of almost 3. This effect can be viewed as resulting from the destructive interference of the emitted photon with itself upon reflecting off the substrate [40-42].

In addition to modifying the lineshape and radiative decay rate, the interference with the substrate also makes the reflectance sensitive to exciton dephasing, quantified by the dephasing rate γ_d. Including this effect, Equation (2) changes to [34]:

$$R(\omega) = \frac{\gamma_r^2}{2\tilde{\gamma}\gamma_T} \frac{1}{(\omega - \omega_0)^2 / \tilde{\gamma}^2 + 1} \tag{3}$$

where γ_T and $\tilde{\gamma}$ are the total decay rate ($\gamma_T = \gamma_r + \gamma_{nr}$) and the total dephasing rate ($\tilde{\gamma} = \gamma_d + \gamma_T / 2$), respectively, while γ_d is the pure dephasing rate.

This effect is analyzed quantitatively using a master equation approach, which also takes into account multiple reflections between the monolayer and the substrate using a transfer matrix method [34,36]. The results of this analysis are in excellent agreement with experimental observations (Fig. 2(b) and Fig. S1 [34]). By fitting the experimental spectra in Fig. 2(a), we can determine the reflectance of the $MoSe_2$ monolayer itself and extract its optical parameters, including radiative, non-radiative decay, and dephasing rates at each temperature: this is because the asymmetric lineshape, which contains information about both the magnitude and phase of the $MoSe_2$ reflection, is affected differently by these rates (Fig. S1(c) in [34]). Figure 2(b) shows deconvolved reflectance spectra of the $MoSe_2$ monolayer in **M2** at various temperatures. The peak reflectance at the exciton resonance reaches 0.85 at 4 K and remains larger than 0.8 below ~40 K (Fig. 2(c)). The total linewidth increases with increasing temperature (Fig. 2(c)). The extracted vacuum radiative linewidth ($\hbar\gamma_r$) of the $MoSe_2$ monolayer **M2** is ~4.0 meV and is almost independent of temperature (Fig. 2(d)). In contrast, both non-radiative decay and pure dephasing have a strong temperature dependence: at 4 K, pure dephasing is less prominent than non-radiative decay, and both are an order of magnitude smaller than the radiative linewidth. Their contributions to the linewidth become larger than the radiative linewidth as the temperature rises above 100 K. We note that $\hbar\gamma_r$ varies from 2 to 4 meV for different monolayers, in agreement with recent experimental studies [16,21,43,44]. This variation may result from

charge/strain inhomogeneity and difference in dielectric environments for different monolayer samples [45].

We now turn to the behavior of our devices, at T=4K, as a function of incident laser power. When a continuous-wave (CW) laser is used as the excitation source (Fig. 3(a)), the reflectance of the device **M2** exhibits sudden jumps and prominent hysteresis as the laser is red-detuned from the exciton resonance. The threshold power at which the reflectance jump occurs becomes larger as the detuning is increased further to the red of the exciton resonance (Fig. 3(a)). When the wavelength of the CW laser beam is blue-detuned above the exciton resonance, the reflectance does not show any hysteresis, and, for high enough power, approaches the bare hBN-SiO_2-Si reflectance. Time-resolved measurements with an electro-optic modulator show that the reflectance jumps occur on a nanosecond timescale (Fig. S2 [34]).

We also explore power-dependent nonlinearities using pulsed excitation (6-ps full width at half maximum). As shown in Fig. 4, the observed nonlinear response is different from that obtained using CW excitation. First, the reflectance jumps and hysteresis completely disappear with the picosecond laser excitation. Second, the power dependence of the asymmetric lineshape also changes. When the wavelength of the picosecond laser is tuned to the blue side of dip (Fig. 4(a)), the **M2** reflectance exhibits an initial decrease followed by a 10-fold increase with increasing peak laser power (I_p). Figure 4(b) shows a two-dimensional plot of the device reflection as a function of incident wavelength and power, demonstrating a blueshift of the reflectance dip. At very large I_p (~1 W), the reflectance eventually converges to that of the hBN-SiO_2-Si reflectance (Fig. 4(a)).

The power-dependent reflectance nonlinearity may originate from exciton-exciton interactions or laser-induced heating. The reflectance jumps and hysteresis observed in Fig. 3(a)

upon CW excitation occur on the time scale of a few nanoseconds [34], much longer than the exciton lifetime. Therefore, it is unlikely for the nonlinearity to be caused by exciton-exciton interactions. Instead, the nonlinearity can be qualitatively explained in terms of the redshift of the exciton resonance resulting from laser-induced heating, Fig. 2(b) [34]. With increasing CW laser power, the exciton density increases, and the non-radiative channels lead to an increase in the monolayer temperature. When the laser wavelength is red detuned from the exciton resonance, this temperature increase brings the exciton resonance closer to the laser wavelength (Fig. 2(b)), giving rise to increased absorption. Such positive feedback leads to the reflectance jump observed in Fig. 3(a). Once the resonance is moved to match the excitation wavelength, it is locked in its energy even at weaker excitation power, leading to hysteresis. As shown in Fig. 3(b), this simple model, in combination with the temperature-induced resonance shift in Fig. 2(b) and non-radiative rates determined in Fig. 2(d), qualitatively explains the experimental data. We note that this model does not take into account the temperature dependence of the heat capacity or thermal conductivity of $MoSe_2$, which may contribute to some discrepancies with the data. The increase in temperature estimated based on the redshift in Fig. 3(a) is consistent with a finite element simulation of our device temperature with the relevant parameters (Fig. S3 [34]).

The power-dependence of the reflection in the picosecond regime (Fig. 4) cannot be explained by laser-induced heating. First, as shown in Fig. 4(b), the dip in the reflectance spectra blueshifts as the laser power increases, in clear contrast to the temperature-induced redshift observed in Fig. 2(a). Second, the time scale of the laser pulse (6 ps) during which this blueshift happens is much faster than the time scale associated with the thermally-induced process in Fig. 3 (~1 ns), while the time interval between the pulses (12.5 ns) is much longer.

Instead, this ultra-fast nonlinearity is likely associated with exciton-exciton interactions. These can give rise to a density-dependent blueshift as well as collisional broadening of the exciton resonance [46]. We model these exciton interaction effects by introducing the density-dependent blueshift of the exciton resonance $\Delta(n) = an$, the change in the dephasing rate $\delta\gamma_d(n) = bn$, and the change in the non-radiative decay rate $\delta\gamma_{nr}(n) = cn$, where n denotes the exciton density [34]. By fitting this model to experimental data, we extract the three parameters related to exciton interactions: $\hbar a = 9.6\times10^{-13}$ meV·cm^2, $\hbar b = 9.4\times10^{-13}$ meV·cm^2, and $\hbar c = 4.0\times10^{-13}$ meV·cm^2. These values indicate that an energy shift equal to the radiative linewidth occurs when excitons are separated by ~8 nm. The results of this analysis, displayed in Fig. 4(c), are in good agreement with experimental observations. The observed shifts are consistent with the theoretical estimates for exchange interactions, $a_{thoery} \sim E_B R^2 \sim 5\times10^{-12}$ meV·cm^2 [47,48], where $E_B \approx 500$ meV is the exciton binding energy and R (~1 nm) denotes the exciton Bohr radius. Detailed understanding of the observed nonlinearities, including the interplay between shifts and dephasing requires additional theoretical and experimental studies.

In summary, our observations demonstrate the remarkable optical quality of hBN-passivated $MoSe_2$ monolayers, as indicated by the radiative decay rate being more than 20 times larger than the non-radiative and pure dephasing decay rates (Fig. 2(d)). This is in clear contrast to excitons in other solid-state systems. For instance, for excitons in high-quality GaAs quantum wells, non-radiative linewidths [49] and disorder-induced inhomogeneous broadening are typically much larger than radiative linewidths [50], preventing efficient reflection.

Our observations open up intriguing prospects for exploring novel phenomena and device applications based on TMD excitons. Such applications may include engineering of robust, long-lived optical edge states using periodically modulated Moiré heterostructures in an external

magnetic field [12,13], controlling the emission patterns of localized sources using atomically thin metasurfaces [10] and realization of quantum nonlinear optical systems featuring broadband optical squeezing [11] or strong interaction between photons [10]. Finally, engineering of the exciton optical response using broad-band reflectors (Fig. 2(a)) or other properly designed photonic systems can be explored to further enhance nonlinearities [34]. Technologically, atomically thin mirrors have intriguing potential. The electrical tunability can enable its use as a reconfigurable component in optical and optoelectronic systems including modulators, active cavities and metasurfaces. Strong, fast, intrinsic and engineered nonlinearities make these systems excellent candidates for realizing optoelectronic devices with possible applications in classical and quantum information processing.

ACKOWLEDGEMENTS

We acknowledge support from the DoD Vannevar Bush Faculty Fellowship (N00014-16-1-2825), AFOSR MURI (FA9550-12-1-0024 and FA9550-17-1-0002), NSF (PHY-1506284), NSF CUA (PHY-1125846), ARL (W911NF1520067), the Gordon and Betty Moore Foundation, and Samsung Electronics. Film deposition and device fabrication was performed at the Harvard Center for Nanoscale Systems.

REFERENCES

[1] J. D. Joannopoulos, S. G. Johnson, J. N. Winn, and R. D. Meade, *Photonic Crystals: Molding the Flow of Light* (Princeton University Press, 2011).

[2] B. E. Saleh and M. C. Teich, *Fundamentals of Photonics* (Wiley New York, 1991).

[3] D. Englund, A. Faraon, I. Fushman, N. Stoltz, P. Petroff, and J. Vuckovic, Controlling cavity reflectivity with a single quantum dot, Nature **450**, 857 (2007).

[4] D. E. Chang, A. S. Sørensen, E. A. Demler, and M. D. Lukin, A single-photon transistor using nanoscale surface plasmons, Nature Phys. **3**, 807 (2007).

[5] K. Hennessy, A. Badolato, M. Winger, D. Gerace, M. Atature, S. Gulde, S. Falt, E. L. Hu, and A. Imamoglu, Quantum nature of a strongly coupled single quantum dot-cavity system, Nature **445**, 896 (2007).

[6] D. O'Shea, C. Junge, J. Volz, and A. Rauschenbeutel, Fiber-optical switch controlled by a single atom, Phys. Rev. Lett. **111**, 193601 (2013).

[7] J. Thompson, T. Tiecke, N. de Leon, J. Feist, A. Akimov, M. Gullans, A. Zibrov, V. Vuletić, and M. Lukin, Coupling a single trapped atom to a nanoscale optical cavity, Science **340**, 1202 (2013).

[8] A. Sipahigil *et al.*, An integrated diamond nanophotonics platform for quantum-optical networks, Science **354**, 847 (2016).

[9] R. J. Bettles, S. A. Gardiner, and C. S. Adams, Enhanced optical cross section via collective coupling of atomic dipoles in a 2D array, Phys. Rev. Lett. **116**, 103602 (2016).

[10] E. Shahmoon, D. S. Wild, M. D. Lukin, and S. F. Yelin, Cooperative resonances in light scattering from two-dimensional atomic arrays, Phys. Rev. Lett. **118**, 113601 (2017).

[11] S. Zeytinoglu, C. Roth, S. Huber, and A. Imamoglu, Atomically thin semiconductors as nonlinear mirrors, arXiv:1701.08228 (2017).

[12] F. Wu, T. Lovorn, and A. H. MacDonald, Topological cxciton bands in Moiré heterojunctions, Phys. Rev. Lett. **118**, 147401 (2017).

[13] J. Perczel, J. Borregaard, D. E. Chang, H. Pichler, S. F. Yelin, P. Zoller, and M. D. Lukin, Topological Quantum Optics in Two-Dimensional Atomic Arrays, Physical Review Letters **119**, 023603 (2017).

[14] K. F. Mak, C. Lee, J. Hone, J. Shan, and T. F. Heinz, Atomically thin MoS_2: A new direct-gap semiconductor, Phys. Rev. Lett. **105**, 136805 (2010).

[15] A. Splendiani, L. Sun, Y. Zhang, T. Li, J. Kim, C.-Y. Chim, G. Galli, and F. Wang, Emerging photoluminescence in monolayer MoS_2, Nano Lett. **10**, 1271 (2010).

[16] G. Moody *et al.*, Intrinsic homogeneous linewidth and broadening mechanisms of excitons in monolayer transition metal dichalcogenides, Nat. Commun. **6**, 8315 (2015).

[17] K. F. Mak, K. He, C. Lee, G. H. Lee, J. Hone, T. F. Heinz, and J. Shan, Tightly bound trions in monolayer MoS_2, Nature Mater. **12**, 207 (2013).

[18] J. S. Ross *et al.*, Electrical control of neutral and charged excitons in a monolayer semiconductor, Nature Communications **4**, 1474 (2013).

[19] B. Ganchev, N. Drummond, I. Aleiner, and V. Fal'ko, Three-particle complexes in two-dimensional semiconductors, Phys. Rev. Lett. **114**, 107401 (2015).

[20] A. Chernikov, A. M. van der Zande, H. M. Hill, A. F. Rigosi, A. Velauthapillai, J. Hone, and T. F. Heinz, Electrical Tuning of Exciton Binding Energies in Monolayer WS_2, Physical Review Letters **115**, 126802 (2015).

[21] M. Sidler, P. Back, O. Cotlet, A. Srivastava, T. Fink, M. Kroner, E. Demler, and A. Imamoglu, Fermi polaron-polaritons in charge-tunable atomically thin semiconductors, Nature Phys. **13**, 255 (2017).

[22] C. R. Dean *et al.*, Boron nitride substrates for high-quality graphene electronics, Nature Nanotech. **5**, 722 (2010).

[23] Y. Zhou *et al.*, Probing dark excitons in atomically thin semiconductors via near-field coupling to surface plasmon polaritons, Nat Nano **12**, 856 (2017).

[24] A. A. Obafunso *et al.*, Approaching the intrinsic photoluminescence linewidth in transition metal dichalcogenide monolayers, 2D Materials **4**, 031011 (2017).

[25] F. Cadiz *et al.*, Excitonic Linewidth Approaching the Homogeneous Limit in MoS_2-Based van der Waals Heterostructures, Physical Review X **7**, 021026 (2017).

[26] A. Chernikov, C. Ruppert, H. M. Hill, A. F. Rigosi, and T. F. Heinz, Population inversion and giant bandgap renormalization in atomically thin WS2 layers, Nat Photon **9**, 466 (2015).

[27] W. Zhao, Z. Ghorannevis, L. Chu, M. Toh, C. Kloc, P.-H. Tan, and G. Eda, Evolution of Electronic Structure in Atomically Thin Sheets of WS2 and WSe2, ACS Nano **7**, 791 (2013).

[28] A. M. Jones *et al.*, Optical generation of excitonic valley coherence in monolayer WSe2, Nat Nano **8**, 634 (2013).

[29] A. M. Jones, H. Yu, J. S. Ross, P. Klement, N. J. Ghimire, J. Yan, D. G. Mandrus, W. Yao, and X. Xu, Spin-layer locking effects in optical orientation of exciton spin in bilayer WSe2, Nat Phys **10**, 130 (2014).

[30] A. Grant, Y. Hongyi, W. Sanfeng, Y. Jiaqiang, G. M. David, C. David, Y. Wang, and X. Xiaodong, Many-body effects in nonlinear optical responses of 2D layered semiconductors, 2D Materials **4**, 025024 (2017).

[31] Y. Li *et al.*, Measurement of the optical dielectric function of monolayer transition-metal dichalcogenides: MoS_2, $MoSe_2$, WS_2 and WSe_2, Physical Review B **90**, 205422 (2014).

[32] M. M. Glazov, T. Amand, X. Marie, D. Lagarde, L. Bouet, and B. Urbaszek, Exciton fine structure and spin decoherence in monolayers of transition metal dichalcogenides, Physical Review B **89**, 201302 (2014).

[33] P. Y. Yu and M. Cardona, *Fundamentals of Semiconductors* (Springer-Verlag Berlin Heidelberg New York, Berlin, 2003), 3rd edn., Graduate Texts in Physics.

[34] See Supplemental Material at http://link.aps.org/ for additional details regarding experimental methods, modelling of the reflection due to TMD monolayers, temperature dependence of nonradiative and dephasing rates, and the analysis of the non-linear response. It includes Refs. [35-38].

[35] P. J. Zomer, M. H. D. Guimarães, J. C. Brant, N. Tombros, and B. J. van Wees, Fast pick up technique for high quality heterostructures of bilayer graphene and hexagonal boron nitride, Appl. Phys. Lett. **105**, 013101 (2014).

[36] H. A. Macleod, *Thin-Film Optical Filters* (CRC press, 2001).

[37] K. S. Gavrichev, V. L. Solozhenko, V. E. Gorbunov, L. N. Golushina, G. A. Totrova, and V. B. Lazarev, Low-temperature heat capacity and thermodynamic properties of four boron nitride modifications, Thermochimica Acta **217**, 77 (1993).

[38] E. K. Sichel, R. E. Miller, M. S. Abrahams, and C. J. Buiocchi, Heat capacity and thermal conductivity of hexagonal pyrolytic boron nitride, Physical Review B **13**, 4607 (1976).

[39] E. M. Purcell, H. C. Torrey, and R. V. Pound, Resonance absorption by nuclear magnetic moments in a solid, Phys. Rev. **69**, 37 (1946).

[40] C. Weisbuch, M. Nishioka, A. Ishikawa, and Y. Arakawa, Observation of the coupled exciton-photon mode splitting in a semiconductor quantum microcavity, Phys. Rev. Lett. **69**, 3314 (1992).

[41] M. Hübner, J. Kuhl, T. Stroucken, A. Knorr, S. W. Koch, R. Hey, and K. Ploog, Collective effects of excitons in multiple-quantum-well Bragg and anti-Bragg structures, Phys. Rev. Lett. **76**, 4199 (1996).

[42] S. Haas *et al.*, Intensity dependence of superradiant emission from radiatively coupled excitons in multiple-quantum-well Bragg structures, Phys. Rev. B **57**, 14860 (1998).

[43] M. Selig *et al.*, Excitonic linewidth and coherence lifetime in monolayer transition metal dichalcogenides, Nat. Commun. **7**, 13279 (2016).

[44] S. Dufferwiel *et al.*, Exciton–polaritons in van der Waals heterostructures embedded in tunable microcavities, Nature communications **6** (2015).

[45] Y. Lin, X. Ling, L. Yu, S. Huang, A. L. Hsu, Y.-H. Lee, J. Kong, M. S. Dresselhaus, and T. Palacios, Dielectric screening of excitons and trions in single-layer MoS2, Nano letters **14**, 5569 (2014).

[46] C. Ciuti, V. Savona, C. Piermarocchi, A. Quattropani, and P. Schwendimann, Role of the exchange of carriers in elastic exciton-exciton scattering in quantum wells, Phys. Rev. B **58**, 7926 (1998).

[47] G. Rochat, C. Ciuti, V. Savona, C. Piermarocchi, A. Quattropani, and P. Schwendimann, Excitonic Bloch equations for a two-dimensional system of interacting excitons, Phys. Rev. B **61**, 13856 (2000).

[48] V. Shahnazaryan, I. Iorsh, I. A. Shelykh, and O. Kyriienko, Exciton-exciton interaction in transition-metal dichalcogenide monolayers, Physical Review B **96**, 115409 (2017).

[49] S. V. Poltavtsev, Y. P. Efimov, Y. K. Dolgikh, S. A. Eliseev, V. V. Petrov, and V. V. Ovsyankin, Extremely low inhomogeneous broadening of exciton lines in shallow (In,Ga)As/GaAs quantum wells, Solid State Commun. **199**, 47 (2014).

[50] S. V. Poltavtsev and B. V. Stroganov, Experimental investigation of the oscillator strength of the exciton transition in GaAs single quantum wells, Physics of the Solid State **52**, 1899 (2010).

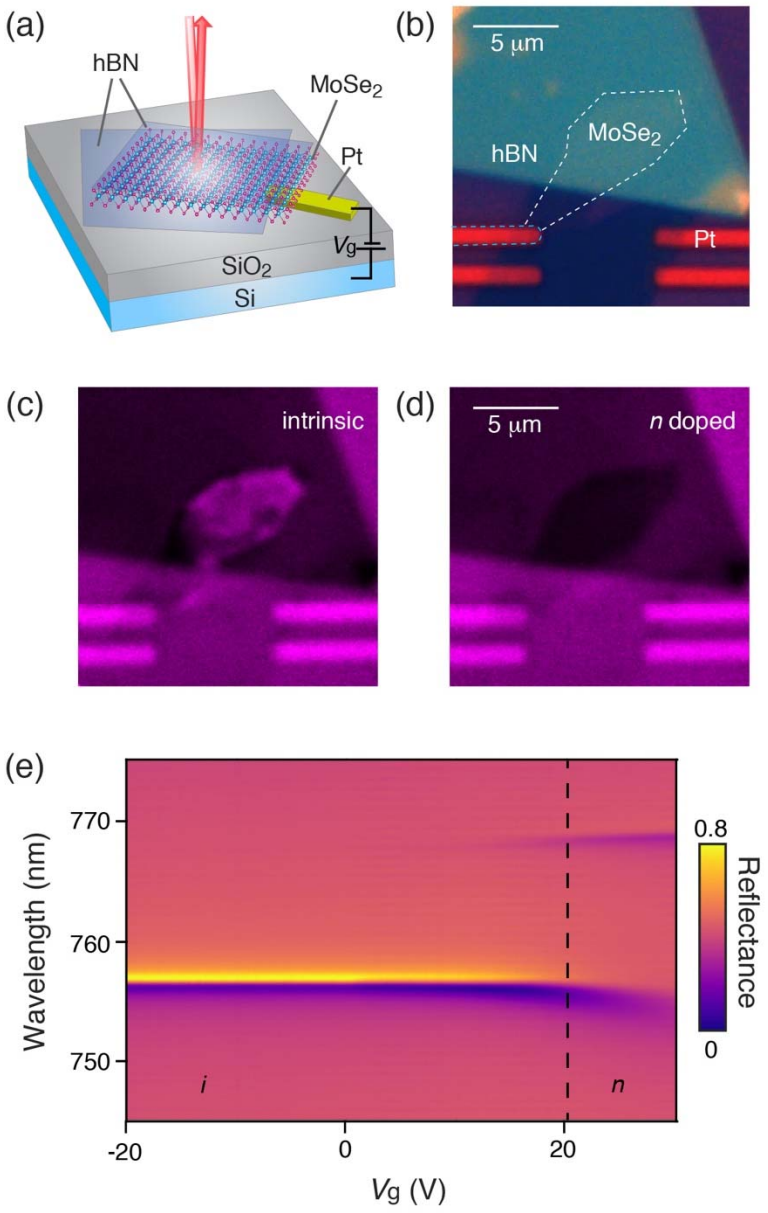

FIG. 1. **Electrically switchable, atomically thin mirror.** (a) Schematic of the experimental setup. A $MoSe_2$ monolayer encapsulated between two hBN layers is placed on SiO_2 (285 nm)/Si substrates. Platinum (Pt) electrodes are used to contact the $MoSe_2$ monolayer, while Si is used as back gate. The incident light resonant with the exciton transitions in $MoSe_2$ can be strongly reflected. The free carrier density in $MoSe_2$ can be tuned with a gate voltage applied to the Si back gate. (b) Optical image of a monolayer $MoSe_2$ device **M1**. The dashed white and blue lines

show the outline of $MoSe_2$ and a Pt contact, respectively. (c) and (d) Reflection images of **M1** under 750-nm resonant laser illumination with a gate voltage of **(**c**)** = -20 V and **(**d**)** 30 V at T = 4 K. The fully encapsulated $MoSe_2$ region shows substantial reflection, while the part that is not fully encapsulated is not as reflective. (e) Reflection spectra of another monolayer $MoSe_2$ device **M2** as a function of gate bias at 4 K. Reflection due to charged excitons can be observed in the electron-doped regime. To obtain absolute reflectance, we normalize the reflected intensity using the measured reflectance of the bare substrate and metal electrodes.

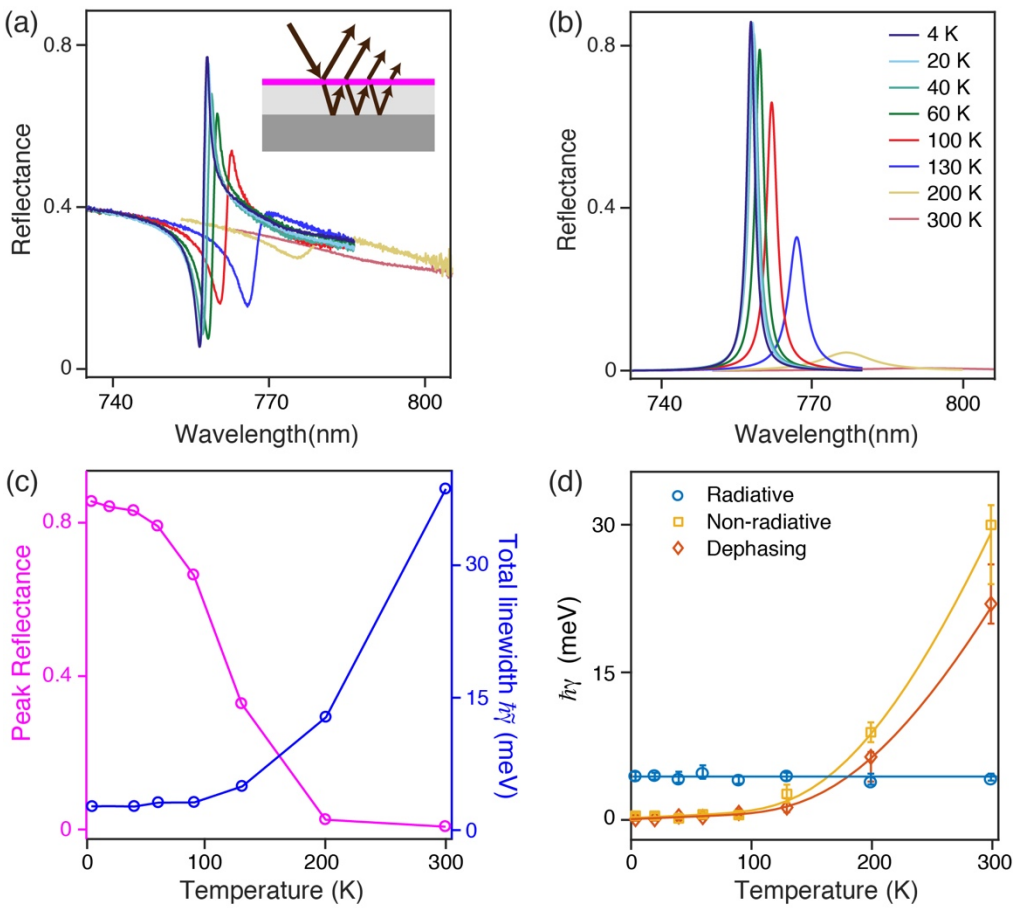

FIG. 2. Temperature-dependent reflectance spectra of a $MoSe_2$ monolayer. (a) Temperature dependent reflection spectra of the monolayer $MoSe_2$ device **M2**. The line colors correspond to different temperatures listed in (b). (b) Reflectance spectra of the $MoSe_2$ monolayer as a function of temperature obtained from the fit. Inset: schematic of interference between the reflection from the $MoSe_2$ monolayer and the reflection of the BN/SiO2/Si substrate (c) Temperature dependence of peak reflectance and total linewidth of the $MoSe_2$ monolayer in **M2**. (d) Radiative, non-radiative and pure dephasing linewidths of the same monolayer as a function of temperature.

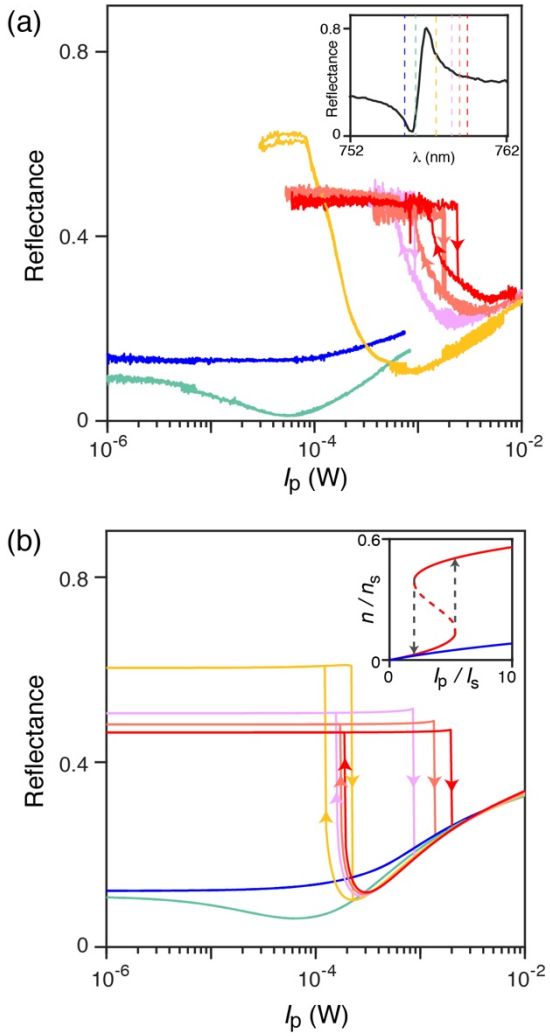

FIG. 3. Nonlinearity of the reflection from a $MoSe_2$ monolayer at T=4K under continuous-wave (CW) resonant excitation. (a) Reflectance of the monolayer $MoSe_2$ device **M2** as a function of the CW laser power (I_p) at different detuning wavelengths, as indicated in the inset. (b) Nonlinear reflectance predicted by the thermal model [34] at different detuning wavelengths. Inset: schematic of the optical bistability with red detuning. Here, n_s and I_s denote the photon density and the incident laser peak power when the energy shift of the exciton transition is equal to the radiative linewidth.

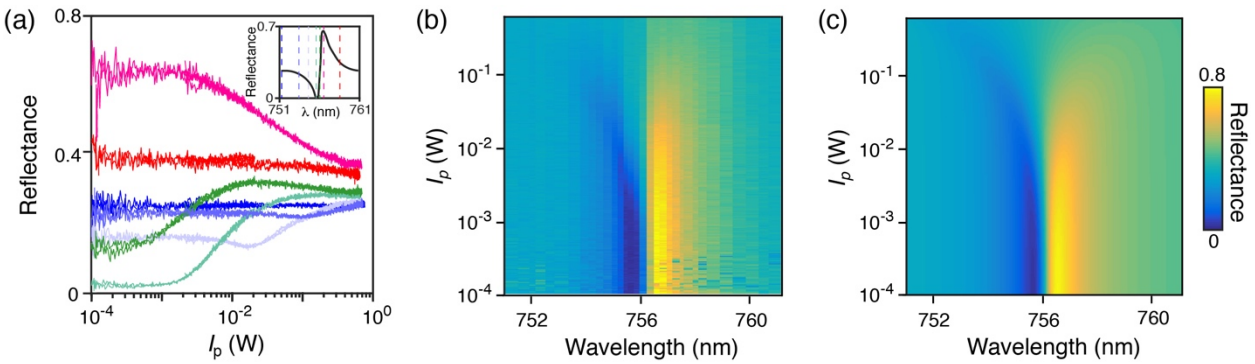

FIG. 4. Nonlinearity of the optical response at T=4K under pulsed-laser excitation. (a) Reflection as a function of peak power (I_p) of the picosecond laser excitation (6ps full width at half maximum), at the wavelengths indicated in the inset. (b) and (c) 2D plots of **(**b**)** experimental and (c) theoretical reflectance at various excitation wavelengths as a function of laser peak power.